OPTICAL PRESCRIPTION OF THE HST

D. REDDING, S. SIRLIN and A. BODEN
Jet Propulsion Laboratory,
California Institute of Technology

J. MO and R. HANISCH
Space Telescope Science Institute

and

L. FUREY
Optical Archaeology, Inc.

Abstract. The optical prescription of the Hubble Space Telescope is estimated by prescription retrieval from defocused WF/PC-II images. New formulas relating the HST primary mirror conic constant and spherical aberration are presented. These new formulas reconcile long-standing differences between estimates of the conic constant derived from phase retrieval and estimates derived by other means.

1. Introduction

The optical prescription of the Hubble Space Telescope — in particular the conic constant of the primary mirror — received a lot of attention following discovery of the spherical aberration of the primary mirror. The concern then was to design appropriate corrective optics for WF/PC-II and COSTAR. This concern remains today, though at a different level, for builders of future instruments, especially of instruments that might seek to compensate for primary mirror (PM) aberrations on a finer spatial scale (Malbet, 1995).

Under the Hubble Aberration Recovery Program (HARP), several groups independently determined estimates of the PM conic (Moore, 1991). Complete agreement among the groups was not achieved. Those who examined the fabrication and test hardware (the fossil data study) derived a number for the PM conic K of -1.01377 ± 0.0003 (Furey, 1993). Several more groups who employed phase retrieval techniques derived numbers ranging from -1.0137 to -1.0150 (e.g. Fienup, 1993; Roddier, 1993; Shao, 1991). The official estimate used to build COSTAR (-1.0139) averaged results from several studies, but did not resolve the differences. These differences were emphasized again recently, with publication of phase retrieval results from WF/PC-II data indicating a value for the primary mirror conic constant of -1.0144 (Krist, 1995).

Also as part of the HARP effort, a direct prescription retrieval technique was developed and applied (Redding, 1993). Like phase retrieval, prescription retrieval is an image inversion parameter estimation approach, where a computer model of the optical system is used to generate simulated images that are matched iteratively

with data images. The HARP prescription retrieval results agreed with the fossil data studies, with an estimate of -1.01398 ± 0.0002.

Prescription retrieval differs from phase retrieval in the parameterization of the image inversion problem. It uses a hybrid ray-trace and diffraction modeling code to solve directly for the conic constant and other prescription parameters. By contrast, phase retrieval techniques solve for intermediate parameters wavefront phase parameters, usually Zernike polynomials. The effect of the conic constant error appears as spherical aberration, or the 11th Zernike polynomial coefficient (Z_{11}) in the 33%-obscured form used by most HST investigators. In a crucial step, the conic constant is then estimated from Z_{11} using a simple formula derived using ray-trace techniques (Furey, 1991).

In this paper, we report new results using prescription retrieval to estimate the PM conic from WF/PC-II focus run images. These preliminary results agree with the HARP fossil data and prescription retrieval results. They disagree with reported estimates of PM conic derived from phase retrieval results using the old formula.

To resolve these differences, we reexamine the formula used to compute conic constant from Z_{11}. Using higher ray densities than was possible originally, and computing formulas for each camera separately, new formulas are derived. These formulas are used to reprocess the spherical aberration results reported by the phase retrieval studies. The resulting estimates of conic constant are in agreement with the earlier official estimate. Combining all results (reprocessed phase retrieval, fossil data and prescription retrieval), the primary mirror conic constant is estimated to be -1.0139±0.0002.

The HST prescription is also of interest for image restoration purposes. We use prescription-based PSF generation codes to support spatially variant PSF image restoration (Redding, 1994; Boden, 1995). Prescription retrieval is used to obtain the accurate prescription data needed to generate representative PSFs.

2. Prescription Retrieval

The HST Optical Telescope Assembly (OTA) consists of a primary and a secondary mirror, plus supports and baffles, forming a Ritchey-Chretien telescope (Burrows, 1990) (Fig. 1). The WF/PC imaging camera optics follow the OTA optics, beginning with a pickoff mirror (POM) at the center of the OTA field of view (Burrows, 1995). Then comes the filter wheel and a pyramid mirror, which splits the field of view into 4 separate cameras. Within each camera there is a fold mirror followed by the WF/PC repeater optics. These consist of a repeater primary (RPM), secondary mirror (RSM), and CCD detector assembled together in a barrel structure. Field curvature is corrected by a plano-concave field flattener lens mounted immediately in front of the detector.

In WF/PC-II, the pupil is reimaged at the RSM, which is figured to compensate for the spherical aberration of the OTA primary. The WF/PC-II design was frozen before the HARP results were finalized, however. The best estimate of K at the time
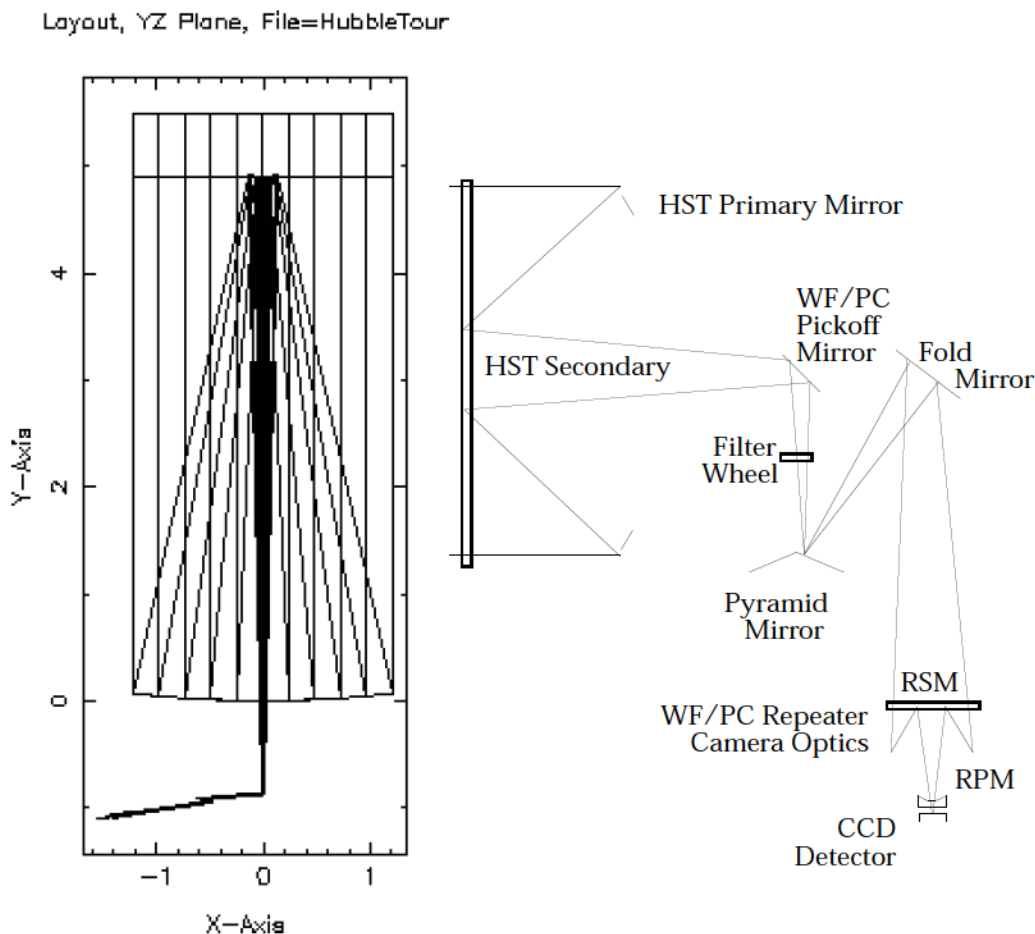
Layout, YZ Plane, File=HubbleTour

Fig. 1.   Ray-trace of the HST and WF/PC.

the RSM design was frozen was -1.0135, so this is the value that the compensation was designed to null. Later results showed the primary to be slightly more aberrated ($K = -1.0139$). The result is that the WF/PC-II compensation leaves a small residual spherical aberration, which is seen in the data.

The precise footprint of the beam on the WF/PC-II RSM can be adjusted on-orbit by tilting the pick-off mirror and, in PC1, WF3 and WF4, by tilting the camera fold mirrors. Errors in placing the beam on the RSM result in coma in the image.

Focus is adjusted by axial translation of the OTA secondary. The OTA secondary can also be decentered to recollimate the telescope. Small misalignments incurred in fabrication are to be expected in the repeater barrel position and angle, plus all individual optics.

Obscurations affecting the image are incurred at the OTA secondary support spiders and baffles, and at the OTA primary, where 3 small support pads are visible at the edges of the aperture. The entrance aperture is placed about 88 mm ahead of the primary mirror, defining the system stop. There is field-angle dependent vignetting at the filters and at the RSM. The location in the pupil of the RSM obscurations is also strongly dependent on field angle. The amount of light passed by the HST and WF/PC-II system varies by about 15% over the full WF field.

In addition to the shearing obscuration effects, there are induced aberrations and distortion that occur with changes in field angle. Small amounts of coma and astigmatism are seen at the edges of the field.

All of these systematic effects on the HST PSF can be accurately predicted from the optical prescription using a combination of ray-trace and physical optics techniques. Here optical prescription means the data defining the orientation, location, figure and index of each optical element. Prescription-based ray-trace codes can accurately determine the wavefront phase and obscuration patterns induced by changing field angles, changing focus or decenter of the secondary, or by misalignment of any of the other optics in the beam train. This is how optical systems are designed, after all.

Fourier optics diffraction beam propagators can then be used to convert ray-based phase information into a transverse electric complex amplitude matrix describing the diffracted beam. This can be done at multiple points in the beam train, if desired, though here it is sufficient to use a single diffraction propagation, from the exit pupil to the detector. The detected intensity is the modulus squared of the field at the detector, resampled into the CCD pixel resolution. Detection effects, such as charge-transfer blurring, motional blurring and noise can then be added.

This approach to modeling optical instruments is realized in a general-purpose optical modeling code called COMP (Redding, 1992). COMP uses the optical prescription to define the image-forming beam train. It uses a full general ray-trace engine to trace a bundle of rays defined at entrance pupil past each optical, vignetting or obscuring surface. The exit-pupil phases computed by the ray-trace drive a Fourier beam propagator, which computes the diffracted image at the detector.

The COMP model provides means to capture the systematic behavior of the images, provided accurate prescription data is used. In general, the design prescription, or even a prescription incorporating results of ground testing will not capture the full performance of the instrument. Means to improve estimates of prescription parameters beyond pre-launch values are provided by prescription retrieval.

Prescription retrieval is an iterative parameter optimization process (Fig. 2), taking the optical design prescription as a starting point, generating images at particular field and focus settings, and matching these images to data images taken under the same conditions (Redding, 1993). The match is improved by varying selected prescription parameters. Some parameters vary with each image in a set, such as field angle, flux, background, and focus setting. Other parameters are common to a set of images,
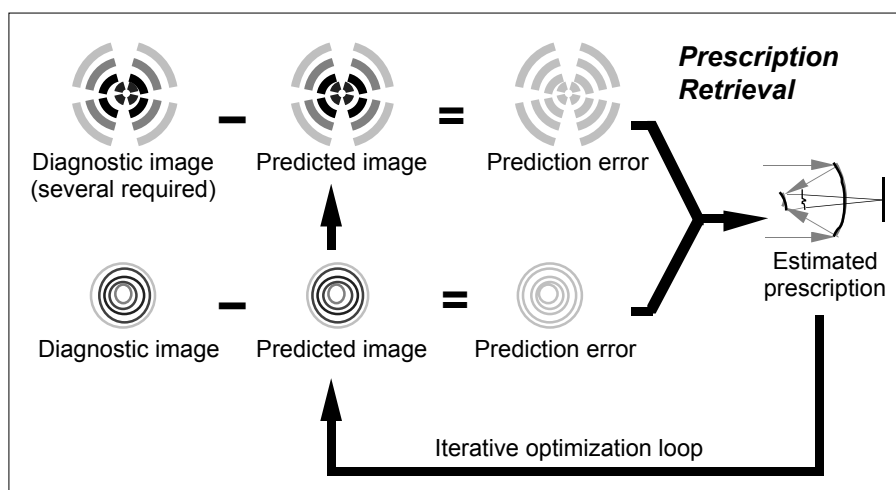
Fig. 2. Sketch of prescription retrieval process.

such as OTA and WF/PC mirror figure parameters, OTA higher-order figure errors, WF/PC barrel alignments, and pickoff mirror and fold mirror tilts.

To get good results for most parameters, a good set of diagnostic images is needed. This should include images taken at multiple focus positions, at multiple field points, and in multiple cameras. Defocusing spreads out the images across many pixels, exposing the signature of the aberrations, such as the spherical aberration rings, and improving the ability to resolve these features. Data taken from both sides of focus resolves ambiguities between asymmetric surface figure aberrations. Defocusing also brings out the obscuration patterns, which help identify alignments. Field diversity shears the effects induced at different surfaces. This was useful in WF/PC-I retrievals, as it separated the aberration centers of the OTA optics from the aberration centers of the repeater cameras: the OTA aberrations remain centered while the camera aberrations shift center with field angle, improving the separability of these contributors to the overall HST spherical aberration.

Prescription retrieval is a better approach than phase retrieval for determining the prescription of an instrument, because it directly solves for the parameters of interest in a model that accurately represents their effect on the data. On the other hand, phase retrieval can be very effective in matching particular images. Zernike polynomials provide a less-constrained, nearly orthonormal phase parameter set compared to prescription parameters. Non-parametric phase retrieval has the further advantage of a very large number of degrees of freedom for matching data.

The problems with phase retrieval have to do with converting the phase information to prescription information (this is discussed in detail later), and in extrapolating fits at one field/focus point to another. Generalizing a match at one point to predict the PSF at another using a conventional physical optics model requires separately identifying and fitting models to all of the systematic variations that occur with

changes in field angle and focus. This includes shearing obscurations, shearing figure errors, and varying aberration and distortion terms. Prescription-based models provide a better basis for predicting these systematic effects.

Either approach can be carried too far, by overfitting the data at high spatial frequencies, so that effects such as scattered light and detection blurring can be incorrectly attributed to optical aberrations. The likelihood of this can be reduced by avoiding scattered or stray light conditions in the data, by including detection blurring in the model, and by using a sufficiently large and diverse data set.

3. WF/PC-II Prescription Retrieval Preliminary Results

This section reports preliminary results of prescription retrieval using WF/PC-II images. Defocused data was taken by the WF/PC-II team soon after the servicing mission. These images were taken on-axis, at 4 focus settings (± 360 μm and ± 180 μm defocus). They were taken in all 4 cameras, using 3 narrow-band filters. Two images were taken for each setting. Cosmic-ray and saturated pixel identification was performed to generate masks for each image. Most results were run with combined images (the 2 images were added), though some were run with single images.

The objective of this first round of retrievals was to determine if the defocused images are consistent with previous estimates of the prescription parameters. The starting prescription was taken to be the WF/PC-II project official as-built Code V prescription. Image-specific parameters varied were field angle, flux, background, and focus setting. System parameters, assumed the same in each image, were the conic constants of the OTA primary and secondary, the conic constants of the repeater camera primary and secondary, WF/PC barrel alignments, and pickoff mirror and fold mirror tilts. In addition, 2 of the runs included Zernike figure errors on the primary mirror. No detection blurring was included in these retrievals.

The individual images were fit fairly well at lower spatial frequencies. The main features for determining the conic constants, namely the bright spherical aberration rings, appear at the same positions. Other features were not matched as well, and we expect that including higher spatial-frequency figure errors and detector blurring will improve the overall match. Figure 3 shows images from PC1 Run 2, comparing simulated and data images for OTA secondary mirror defocus = 360 μm. Figure 4 compares simulated and data images for defocus = 180 μm.

The results for mirror conic constants are summarized in Table I. The initial parameter values for the first 4 runs were set to the as built official estimates. All conics were allowed to vary, together with other image and system parameters. The results show very little change in the estimates of the OTA conic constant parameters. The PC1 repeater conic constant estimates also change very little. This is consistent with test results that show only a very small amount of spherical aberration in the PC1 repeater camera (Krist, 1995). The estimates of the WF2 repeater conics change more significantly; those for WF3 change very little.
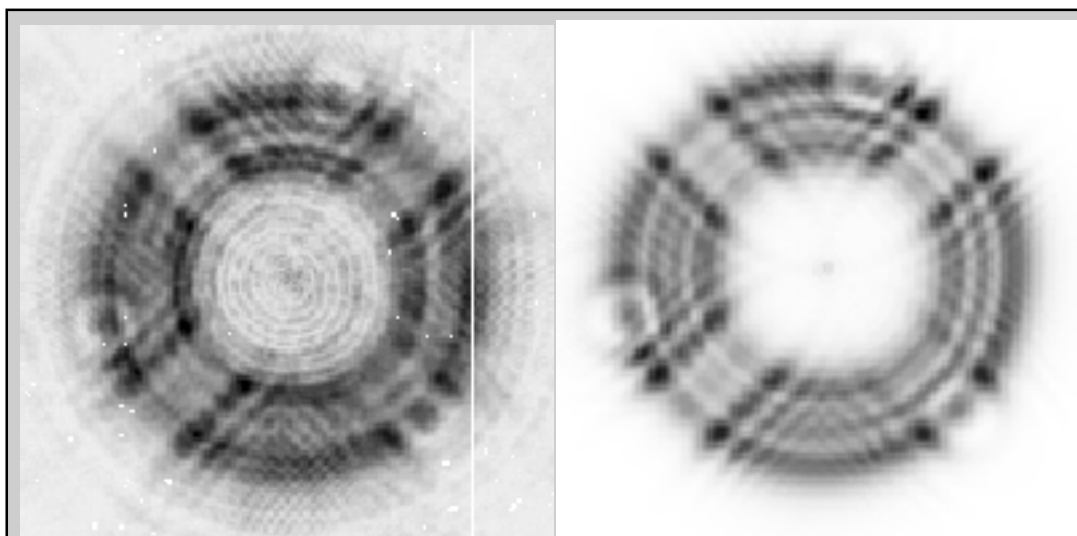
Fig. 3. Data (left) and simulated (right) images from WF/PC-II, PC1 camera (Run 2). Secondary mirror defocus=360 microns; Filter=F502N.
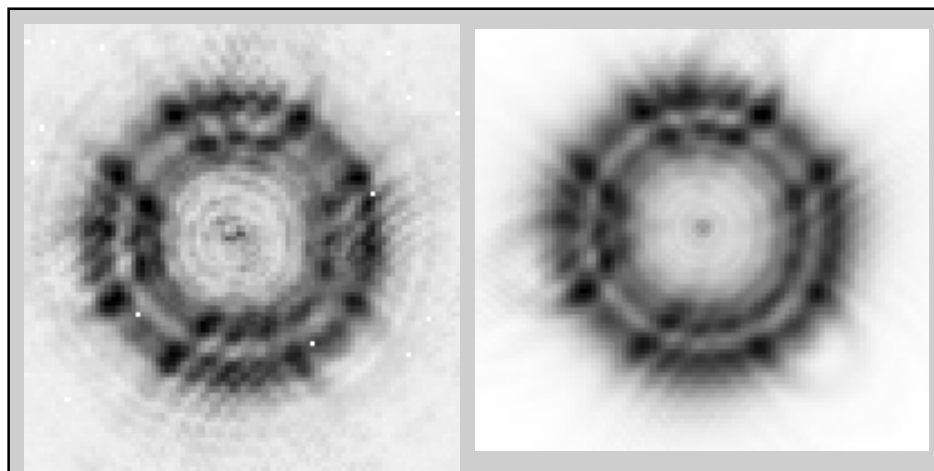

Fig. 4. Data (left) and simulated (right) images from WF/PC-II, PC1 camera (Run 2). Secondary mirror defocus=180 microns; Filter=F502N.

To test the hypothesis that the OTA PM conic is actually less than -1.0139, and to test the separability of the conic parameters, initial values for the last 2 cases were set at lower values (-1.0141 and -1.0144, respectively). The estimates of the OTA PM conic did not converge to the same numbers. The overall spherical aberration remained about the same, however, as the increased spherical aberration from the PM was reduced by changes in the estimated conics for the other cameras (the Z_{11} numbers were fit to OPD maps generated using the retrieved prescriptions). The indication is that this data does not provide sufficient diversity to separate the contributions of figure errors at multiple surfaces. This being the case, the most likely

TABLE I

WF/PC-II prescription retrieval preliminary results.

Parameter	"As-built"	PC1 Run 1	PC1 Run 2	WF2 Run 3	WF3 Run 4	PC1 Run 5	PC1 Run 6
OTA PM K	-1.01390	-1.01390	-1.01390	-1.01390	-1.01390	-1.01408	-1.01434
OTA SM K	-1.49600	-1.49597	-1.49597	-1.49600	-1.49579	-1.49771	-1.50220
PC1 PM K	-0.30599	-0.30601	-0.30599			-0.30507	-0.30386
PC1 SM K	-109.543	-109.517	-109.554			-109.621	-108.254
WF2 PM K	-0.503155			-0.486412			
WF2 SM K	-94.4998			-92.2225			
WF3 PM K	-0.503155				-0.50323		
WF3 SM K	-94.4998				-94.4897		
In-focus Z_{11}		-0.00853				-0.00927	-0.00960

results are those which require the least change in the as built a priori estimates. Runs 1–4 are to be preferred on these grounds. The conclusion is that the data is consistent with the as-built estimates of the OTA prescription.

The diversity in the data set is limited, as all images were taken on-axis in the cameras (not the OTA). The data does not provide displaced aberration centers, which can be useful in separating OTA and repeater figure errors. This is less true for WF/PC-II than WF/PC-I, as the optical correcting scheme places the RSM at a pupil. There is some limited separability due to the fact that changing the OTA PM conic induces astigmatism, as the beam is off-axis in the OTA, whereas changing the repeater conic does not, as it is on axis. Separating RSM figure from the OTA PM figure ultimately requires averaging effects across multiple cameras. We have not yet done a thorough formal error analysis of these estimates and so cannot yet comment quantitatively on the separability of the estimates.

As mentioned earlier, our main interest is in retrieving prescriptions for generating PSFs for image restoration. Most of the retrieval can be done once, using defocused images as above. Some parameters should be retrieved directly from each image to be restored, however. An example is the OTA secondary mirror focus. The HST breathing mode and desorption effects cause drift of the overall telescope focus over time. This is not precisely understood, but the amount of defocus can be determined by running a tweak retrieval using a point source from the image to be restored. Another example is the registration of dithered images, which can be determined by retrieving field angles for the same star(s) on each image separately.

Retrieval from in-focus star images is also the best approach for determining detection blurring. This phenomenon is the position-dependent probability that a photon
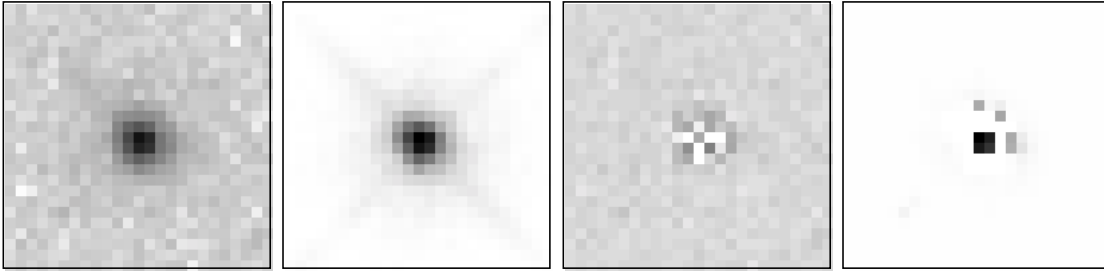
Fig. 5. Data (left), simulated, subtracted and restored images from WF/PC-II, WF3 camera (log10 stretch). Retrieved defocus=6 microns. Retrieved blur kernel=0.79.

hitting a particular pixel will register in an adjacent pixel. It is likely due to charge transfer in the CCD chip, or perhaps to scattering. We use a simple convolution model with a 3×3 kernel function, parameterized by the peak value of the kernel, to represent this effect. The blur kernel value is retrieved from in-focus data.

Figure 5 presents an example of retrieval from an in-focus image. This star appears on a set of 4 WF/PC-II, WF3 images that were combined and restored. The basic prescription was that retrieved from the defocused data (Run 4). The in-focus image data was matched to determine the registration of the frame (pixel 235.269, 524.379), blur kernel peak value (0.79), and image defocus (6 μm). The match is quite good, as evidenced by the subtracted image, which subtracts the simulated from the data images. The restored image is also very good, with no halo of poorly-fit pixels surrounding the core.

4. Computing Conic Constant from Spherical Aberration Data

To convert phase retrieval (not prescription retrieval) results to estimates of the OTA PM conic constant, the following formula has been most widely used (Furey, 1991):

$$K = K_0 + \frac{Z_{11}}{(dZ_{11}/dK)} \tag{1}$$

Here the coefficients are $K_0 = -1.00223$ and $dZ_{11}/dK = 35.30$ in waves at 6328 Å. These coefficients were derived in the OTA only, using a limited resolution ray-trace code. In this section we re-examine this formula, computing new coefficients for each camera separately, using higher ray grid densities. Then we apply the new formulas to the previously reported phase retrieval results to obtain new estimates of the OTA PM conic K.

The procedure followed to generate the coefficients was as follows:

1. The OTA optical prescription was used to generate an OPD map at the exit pupil.
2. The OPD map was fitted with the 33%-obscured Zernike polynomials and the Z_{11} value was recorded.

TABLE II
Z_{11}-to-K conversion coefficients.

	Camera	K_0	dZ_{11}/dK	Ray Sampling	Field Point
1	OTA	-1.00223	35.30	19×19	OTA Axis (original formula)
2	OTA	-1.00223095	35.3157	19×19	OTA Axis
3	OTA	-1.00223096	37.1200	256×256	OTA Axis
4	WF/PC-I PC6	-1.00222368	37.4123	128×128	Camera Axis (Off-axis in OTA)
5	WF/PC-I PC6	-1.00222379	36.9350	256×256	Camera Axis (Off-axis in OTA)
6	WF/PC-I PC6	-1.00227227	39.4485	256×256	OTA Axis (Off-axis in camera)
7	WF/PC-II PC1	-1.01354128	37.1765	256×256	Camera Axis (Off-axis in OTA)
8	WF/PC-II PC1	-1.01354409	36.5523	256×256	OTA Axis (Off-axis in camera)
9	WF/PC-II WF3	-1.01335890	37.0589	256×256	Camera Axis (Off-axis in OTA)

3. The OTA PM K was changed to new values, and steps 1–2 were repeated for each.

4. K was plotted against the derived Z_{11} values over the region of interest, and the linear model above was fit to the curve.

The ray sampling grid used for these coefficients was 19×19. Similar results were obtained using other low-density sampling grids. We have now repeated the same procedure running much larger ray grids, for each camera separately. The results are summarized in Table II.

Row 1 in Table II is the original formula coefficients. Row 2 repeats that case using the COMP code, showing that the results agree. Rows 5, 7 and 9 provide coefficients for the WF/PC-I PC and the WF/PC-II PC and WF cameras, respectively. Note that the K_0 coefficient for the WF/PC-II cameras is at the designed correction value of -1.0135. Rows 6 and 8 show that the conversion at one field angle can differ appreciably from the conversion at another. Row 4 shows sensitivity to sampling density and precise placement of the ray grid on the optics. The lesson from these cases is that these formulas should be used with non-zero error bars! The value of the error bars need not be large for a particular field/focus point in a particular camera. If a single formula is to cover all cameras and conditions, however, the error bar should be about 0.0005.

Using the new camera-specific formulas, Z_{11} estimates derived from phase retrieval and reported by other workers were reprocessed. The results are summarized in Table III. The effect of the new formulas is to increase the estimated K from an averaged value of -1.0144 to an averaged value of -1.01395. This compares to estimates of -1.01377 ± 0.0002 and -1.01398 ± 0.0002 from the HARP fossil data and prescription retrieval studies, respectively. The average of these 3 numbers is -1.01390, and all

TABLE III

Reprocessed phase retrieval estimates of K.

Z_{11}	K by new formula	K as reported	Camera	Formula (Table II)	Reference	Notes
-0.277	-1.01404	-1.0145	FOC	3	Krist, 1995	avg of 3 λs
-0.300	-1.01376	-1.0146	WF/PC-I PC6	5	Krist, 1995	avg of 2 λs
-0.013	-1.01412	-1.0142	WF/PC-II PC1	7	Krist, 1995	avg of 2 λs
-0.020	-1.01395	-1.0143	WF/PC-II WF2	9	Krist, 1995	avg of 2 λs
-0.024	-1.01400	-1.0144	WF/PC-II WF3	9	Krist, 1995	avg of 2 λs
-0.023	-1.01394	-1.0143	WF/PC-II WF4	9	Krist, 1995	avg of 2 λs
-0.290	-1.01369	Not given	WF/PC-I PC6	5	Roddier, 1993	
-0.299	-1.01408	-1.0144	WF/PC-I	5	Fienup, 1993	

of the reprocessed phase retrieval, fossil data, and prescription retrieval results lie within ± 0.0002 of this number.

A word of caution is warranted. Agreement to within ± 0.0002 by averaging does not provide a definitive error bar. Some sources of error were not fully characterized in the various studies. This includes the spherical aberration of the various stimuli used in testing COSTAR and WF/PC-II, which were required to meet less stringent criteria (Furey, 1994). This is significant in deriving Z_{11} by phase retrieval.

5.   Conclusion

We have presented prescription retrieval results indicating that the official as-built estimates of the OTA prescription are consistent with WF/PC-II image data. We also derived new formulas for the conversion of exit-pupil phase to OTA PM conic. These formulas were applied to estimates of the HST spherical aberration obtained by others using phase retrieval techniques. The result was an estimate of the OTA PM conic that agrees with earlier fossil data and prescription retrieval studies. Averaging results from phase retrieval, prescription retrieval and fossil data studies, the OTA PM conic is estimated to be -1.0139 ± 0.0002.

Improving the accuracy of the estimates of the OTA prescription parameters is important for future replacement cameras that might seek to compensate the higher-order aberrations of the OTA primary mirror (Malbet, 1995). OTA PM conic errors at the 0.0005 level could saturate the high actuator density, small stroke deformable mirrors being designed for such a mission. Further work to improve these estimates may be desirable in light of these requirements.

References

A. Boden, D. Redding, J. Mo, R. Hanisch and R. White, "Comparative Results with Massively Parallel Spatially-Variant Maximum Likelihood Image Restoration," Bulle- tin of the American Astronomical Society, V. 27, No. 2, pp. 924-929 (1995).

OTA Handbook Version 1.0, C. Burrows, (Ed.), STScI Publication (May 1990).

Wide Field and Planetary Camera 2 Instrument Handbook , C. Burrows, (Ed.), STScI Publication (June 1995).

J. Fienup, J. Marron, T. Schulz and J. Seldin, "Hubble Space Telescope Characterized by Using Phase Retrieval Algorithms," Applied Optics, V. 32, No. 10 (April 1993).

L. Furey, Derivation of the HST Primary Mirror Conic Constant from Fossil Data, HDOS Report (July 1991).

L. Furey, T. Dubos, D. Hansen and J. Samuels-Schwartz, "Hubble Space Telescope Primary Mirror Characterization by Measurement of the Reflective Null Corrector," Applied Optics, V. 32, No. 10 (April 1993).

L. Furey, Post-FSM Optical Prescription Status Report, HDOS Memo A16-ST-0331 (May 1994).

J. Krist and C. Burrows, "Phase Retrieval Analysis of Pre- and Post-Repair Hubble Space Telescope Images," ST ScI Preprint No. 901 (1995). To appear in Applied Optics.

F. Malbet, J. Yu and M. Shao, High-Dynamic-Range Imaging Using a Deformable Mirror for Space Coronography, PASP, Vol. 107, No. 710 (1995).

D. Moore et al, HIORP Final Report (1991).

D. Redding, M. Lee and S. Sirlin, "Improved Prescription Retrieval and Modeling Code," in The Restoration of HST Images and Spectra II, R. Hanisch and R. White, eds. (1994).

D. Redding, L. Needels, K. Wallace and J. Yu, Controlled Optics Modelling Package User Manual, JPL Document D-9816 (June 1992).

D. Redding, P. Dumont and J. Yu, "Hubble Space Telescope Prescription Retrieval," Applied Optics, V. 32, No. 10 (April 1993).

C. Roddier and F. Roddier, Combined Approach to the Hubble Space Telescope Wavefront Distor- tion Analysis, Applied Optics, V. 32, No. 16 (June 1993).

M. Shao, M. Colavita, R. Dekany, P. Dumont, B. Hines, M. Levine, D. Redding, S. Brewer and A. Decou, "Image Inversion Analysis of Hubble Space Telescope Optics Using a Non-Linear Least-Squares Algorithm," JPL Report (1991).